External light control of three-dimensional ultrashort far-infrared pulses in an inhomogeneous array of carbon nanotubes

Eduard G. Fedorov
ITMO University, 197101 Saint Petersburg, Russia

Alexander V. Zhukov
*Singapore University of Technology and Design, 8 Somapah Road, 487372 Singapore
and Entropique Group Ltd., 3 Spylaw Street, Maori Hill, 9010 Dunedin, New Zealand*

Roland Bouffanais
Department of Mechanical Engineering, University of Ottawa, Ottawa ON K1N 6N5, Canada

Natalia N. Konobeeva
Volgograd State University, 400062 Volgograd, Russia

Evgeniya V. Boroznina
Volgograd State University, 400062 Volgograd, Russia

Boris A. Malomed
*Department of Physical Electronics, School of Electrical Engineering, Faculty of Engineering, Tel Aviv University, 69978 Tel Aviv, Israel
and Instituto de Alta Investigación, Universidad de Tarapacá, Casilla 7D, Arica, Chile*

Hervé Leblond
LUNAM Université, Université d'Angers, Laboratoire de Photonique d'Angers, EA 4464, 2 Boulevard Lavoisier, 49000 Angers, France

Dumitru Mihalache
*Academy of Romanian Scientists, 54 Splaiul Independentei, Bucharest RO-050094, Romania
and Horia Hulubei National Institute of Physics and Nuclear Engineering, Magurele RO-077125, Romania*

Mikhail B. Belonenko
*Volgograd State University, 400062 Volgograd, Russia
and Entropique Group Ltd., 3 Spylaw Street, Maori Hill, 9010 Dunedin, New Zealand*

Nikolay N. Rosanov
*Ioffe Institute, 194021 Saint Petersburg, Russia
and ITMO University, 197101 Saint Petersburg, Russia*

Thomas F. George
*Office of the Chancellor, Departments of Chemistry & Biochemistry and Physics & Astronomy,
University of Missouri-St. Louis, St. Louis, Missouri 63121, USA*

We present a study of the propagation of three-dimensional (3D) bipolar electromagnetic ultrashort pulses in an inhomogeneous array of semiconductor carbon nanotubes (CNTs) in the presence of a control high-frequency (HF) electric field. The inhomogeneity is present in the form of a layer with an increased concentration of conduction electrons, which acts as a barrier for the propagation of ultrashort electromagnetic pulses through the CNT array. The dynamics of the pulse is described by a nonlinear equation for the vector potential of the electromagnetic field (it takes the form of a 3D generalization of the sine-Gordon equation), derived from the Maxwell's equations and averaged over the period of the HF control field. By means of systematic simulations, we demonstrate that, depending on the amplitude and frequency of the HF control, the ultrashort pulse approaching the barrier layer either passes it or bounces back. The layer's transmissivity for the incident pulse is significantly affected by the amplitude and frequency of the HF control field, with the reflection coefficient nearly vanishing in intervals that make up a discrete set of transparency windows, which resembles the effect of the electromagnetically induced transparency. Having passed the barrier, the ultrashort pulse continues

to propagate, keeping its spatiotemporal integrity. The results may be used for the design of soliton valves, with the transmissivity of the soliton stream accurately controlled by the HF field.

I. INTRODUCTION

Modern laser technologies offer a variety of opportunities for generating ultrashort pulses corresponding to several half-periods of field oscillations [1–4]. This has provided the impetus for studies of the formation and propagation of nonlinear electromagnetic waves in various media [5–12]. In this connection, graphene-based materials have attracted attention as promising media for both basic research and practical applications in the fields of photonics and optoelectronics (e.g., see reviews [13,14] and references therein). In particular, carbon nanotubes (CNTs)—quasi-one-dimensional carbon macromolecules [15–17]—offer high potential for the development of optoelectronic devices, based on the propagation of nonlinear electromagnetic waves, such as ultrafast laser pulses. These may be photodetectors, solar energy converters, transparent conductive surfaces, displays, etc.

From the point of view of the potential applications to optoelectronics, interest in carbon nanotubes is due to the peculiarity of their electronic structure. In particular, the nonparabolicity of the dispersion of conduction electrons (the dependence of the energy on the quasimomentum) leads to a significant nonlinearity in the response of nanotubes to the application of a moderate electromagnetic field with intensities starting from $10^3 - 10^4$ V/cm (see. e.g., Ref. [18]). This circumstance makes it possible to observe a number of unique physical phenomena in nanotube media, including nonlinear diffraction, self-focusing of laser beams, propagation of solitons, etc. [19–21].

The possibility of propagation of infrared solitary electromagnetic waves in arrays of CNTs was first theoretically established in the approximation of a uniform field along the axis of nanotubes in a one-dimensional (1D) model in Ref. [21]. Subsequently, the possibility of the propagation and interaction of solitary electromagnetic waves in CNT arrays was studied in a 2D model, using the same approximation as mentioned above [22–24], and taking into account localization of the field in directions orthogonal to the propagation of the electromagnetic wave [25]. In Refs. [26,27], taking into account the most fundamental 3D spatial localization of the laser pulse field, the propagation and interaction of solitary electromagnetic waves in nanotube arrays in the 3D geometry has been studied.

The previous studies have established that the evolution of electromagnetic waves in arrays of semiconductor CNTs substantially depends on various physical factors, such as the presence of various impurities, as well as static and dynamic inhomogeneities. In particular, doping a sample with a uniformly distributed multilevel impurity can lead to a modification of the parameters of a propagating electromagnetic pulse, as compared to the propagation in pure samples [28]. In addition, dynamic inhomogeneities of the spatial distribution of the concentration of conduction electrons in CNT arrays induced by laser pulses can serve as mediators in the interaction

of extremely short pulses [27]. Besides that, the interaction of ultrashort pulses with static localized inhomogeneities in the array deserves special attention from the perspective of possible applications (see, e.g., Ref. [29]). For example, as a result of the interaction of the ultrashort pulses with a layer carrying high electron density (HED), selective nature of the pulse scattering by such a layer has been established, offering new possibilities for developing light control methods in micro- and nanostructures [30–32].

The concept of controlling the dynamics of ultrashort pulses, proposed in recent works, suggests various outcomes of the interaction of a solitary wave with the structural inhomogeneity of the medium, depending on both parameters of the pulse itself and properties of the inhomogeneity. For example, a pulse with an amplitude significantly exceeding a certain threshold value can pass the HED layer, while a pulse with the amplitude falling below the threshold will be reflected from the layer. In this case, decrease in the thickness of the inhomogeneity layer also facilitates the passage of the pulse through such a layer. However, properties of media acting as the waveguides are usually fixed by the manufacturing procedure. Parameters of the laser pulses cannot be easily adjusted either if the pulse stream is generated by a standard source. Therefore, possibilities for the design of the control of the pulse dynamics in micro- and nanostructures are limited, and it is relevant to develop a method for controlling the dynamics of ultrashort pulses in inhomogeneous nonlinear media by means of an independent tool. In this work we demonstrate that externally applied high-frequency (HF) electric field may provide such a tool, which acts by dynamically modifying properties of the electronic subsystem in the CNT array. The control HF field is switched on for a time significantly exceeding the characteristic duration of the extremely short pulse scattered by the HED layer. During the presence of the control HF field, the pulse has the time to enter the system, to adjust its parameters to the properties of the medium—modified by this control HF field—and to interact (i.e., to perform the act of scattering/collision, transmission, or reflection) with the HED layer. The result is the creation of transparency windows at specific values of the amplitude of the control HF field, at which the reflection coefficient practically vanishes. This effect is similar to the well-known phenomenon of the electromagnetically induced transparency [33–35]. Further, turning the external field on/off may allow ultrafast switching of the interaction of ultrashort pulses with the HED layer, which thus acts as a controllable semitransparent mirror for the pulses. As a result, pulses with the same parameters can either pass the layer or bounce back from it, depending on the presence of the HF control field. Thus, in this work we address the dynamics of 3D ultrashort electromagnetic pulses in the bulk array of semiconductor CNTs, with the HED layer embedded into it, which acts as a controllable obstacle for the transmission of pulses through the system.

The rest of the paper is organized as follows. The system is formulated in Sec. II, the basic evolution equation for the electromagnetic field carrying the ultrashort pulse is derived in Sec. III, and characteristics of the field are presented in Sec. IV. Numerical results for the transmission of the pulse in the CNT array and its interaction with the HED layer, in the absence and presence of the HF control field, are systematically reported in Sec. V, where, in particular, the existence of the above-mentioned transparency windows is demonstrated. Finally, main findings of the work are summarized in Sec. VI.

II. SYSTEM

We consider the propagation of a bipolar solitary electromagnetic wave in the bulk array of single-walled semiconductor CNTs, embedded in an inhomogeneous dielectric medium, under the influence of an external HF control electromagnetic field. The vector of the electric field of a bipolar pulse should have opposite directions at different instants of time at a fixed point. It is assumed that space between the CNTs is filled with a dielectric, while the heterogeneity of the array is represented by a layer with an increased concentration of conduction electrons. The CNTs considered here are of the zigzag type $(m, 0)$, where integer m (different from a multiple of three for semiconductor nanotubes) determines the CNT radius, $R = mb\sqrt{3}/2\pi$, where $b = 1.42 \times 10^{-8}$ cm is the distance between adjacent carbon atoms [15–17]. The CNTs are arranged in such a way that their axes are parallel to the common x axis, and an ultrashort laser pulse propagates along the z axis, that is, in a direction perpendicular to CNT axes. In this case, the electric field of the pulse, $\mathbf{E} = \{E, 0, 0\}$, is collinear to the x axis, see Fig. 1. We assume that the overlap of wave functions of electrons between adjacent CNTs is negligible (no tunneling of electrons between adjacent nanotubes), and the system under consideration is electrically quasi-one-dimensional, featuring conductivity only along the x axis.

Further, we assume that, in addition to the field of the ultrashort electromagnetic pulse, the system includes an external control HF electric field $\mathbf{E}_1 = \{E_1, 0, 0\}$, with $E_1 = E_{10}\cos(\omega_1 t + \alpha)$, where E_{10}, ω_1, and α are the amplitude, frequency and phase shift of the control field. We also assume that frequency ω_1 significantly exceeds the inverse of the characteristic pulse's temporal width: $\omega_1 \gg 2\pi/\Delta t_{\text{pulse}}$. HF field $\mathbf{E}_1$ may be realized by exciting transverse standing electromagnetic wave modes of the embedding waveguide, by means of an appropriate laser source.

The CNT array, which is a discrete structure at the microscopic level, is considered in this paper in the approximation of a continuum medium, in the context of the interaction with the electromagnetic pulse and the external HF radiation (the control field). This approximation is valid for a wide range of system's parameters—in particular, when the wavelength of the external HF radiation and the characteristic distance of the variation of the pulse's field substantially exceed the separation between adjacent CNTs, as well as the mean-free path of conduction electrons along the CNT axis. For example, the CNT radius $R \approx 5.5 \times 10^{-8}$ cm and $m = 7$ produce the separation between them (sufficient to ensure the conductivity of in the CNT array only along the x-axis)—even if substantially
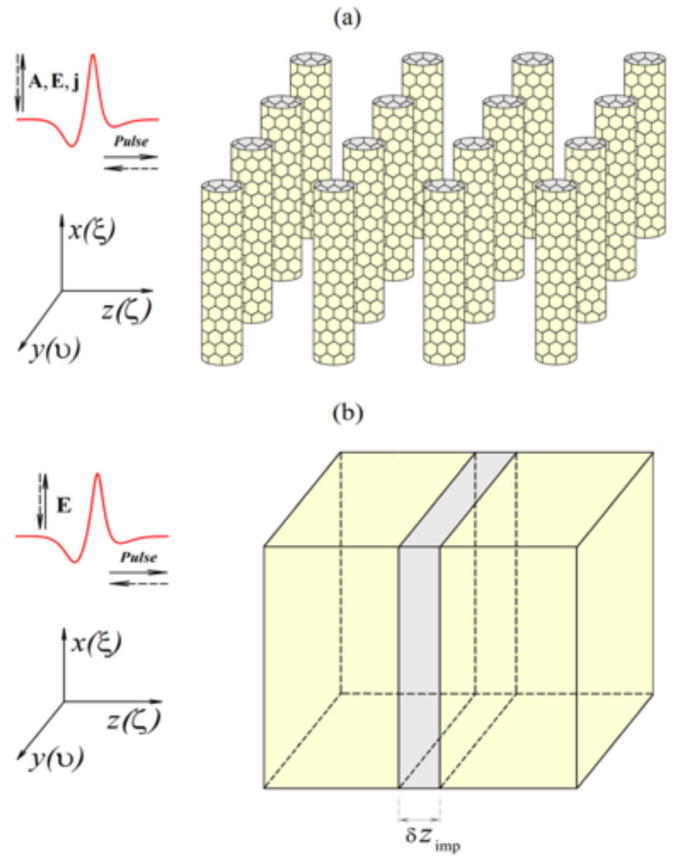

FIG. 1. Geometry of the system: (a) Schematic representation of an array of nanotubes and the orientation of vectors of physical quantities in the Cartesian coordinate system. (b) Location of a layer of increased electron concentration.

exceeding radius R—as negligibly small in comparison with wavelengths of the electromagnetic radiation in the infrared range.

Given the orientation of the coordinate system axes relative to the nanotube axis chosen in Fig. 1, the electron energy spectrum for CNTs takes the form of

$$\epsilon(p_x, s) = \gamma_0\sqrt{1 + 4\cos\left(p_x\frac{d_x}{\hbar}\right)\cos\left(\pi\frac{s}{m}\right) + 4\cos^2\left(\pi\frac{s}{m}\right)},$$

(1)

where $\gamma_0 = 2.7$ eV, the electron quasimomentum is $\mathbf{p} = \{p_x, s\}$, p_x is the projection of the quasimomentum of the conduction electron onto the CNT axis, and s is an integer characterizing the momentum quantization along the perimeter of the nanotube, $s = 1, 2, \ldots, m$. Here m is the number of hexagonal carbon cycles forming the circumference of a nanotube, γ_0 is the overlap integral, and $d_x = 3b/2$ [15–17].

We solve the problem in the semiclassical approximation, thus requiring the following conditions to be satisfied: $\hbar\omega_0 \ll 2\gamma_0$ (ω_0 is the characteristic frequency of the electronic subsystem of CNTs), $|Ee|d \ll 2\gamma_0$, $|E_1 e|d \ll 2\gamma_0$, $\hbar/\Delta t_{\text{pulse}} \ll 2\gamma_0$. We adopt one more important assumption regarding the ratio of the duration of the electromagnetic pulse, Δt_{pulse}, relaxation time t_{rel} of the conduction current along the axis of the nanotubes, and the time interval Δt for observing the evo-

lution of the electromagnetic field in the system. Specifically, we assume that the observation time substantially exceeds the characteristic pulse duration, but is still shorter than the relaxation time: $\Delta t_{\text{pulse}} \ll \Delta t < t_{\text{rel}}$. This condition allows us to maintain the collisionless approximation, in which we can neglect the influence of collisions of electrons with defects of the CNT array on the evolution of the conduction current and pulse's electromagnetic field. It should be noted that typical scattering times are strongly temperature dependent [36], as $t_{\text{rel}} \propto \sinh(1/T)$. Thus, the collisionless approximation may be readily maintained by appropriately cooling the experimental sample.

III. THE EVOLUTION EQUATION FOR THE ELECTROMAGNETIC FIELD OF SHORT PULSES

A. Density of conductivity electrons

Starting from the full system of the Maxwell's equations [37,38], we derive the following wave-propagation equation, in the geometry under the consideration:

$$\frac{\varepsilon}{c^2}\frac{\partial^2 A}{\partial t^2} - \frac{\partial^2 A}{\partial y^2} - \frac{\partial^2 A}{\partial z^2} - \frac{4\pi}{c}j = 0, \qquad (2)$$

where $A(x, y, z, t)$ and $j(x, y, z, t)$ are the projections of the vector potential $\mathbf{A} = \{A, 0, 0\}$ and current density $\mathbf{j} = \{j, 0, 0\}$ onto the x axis, and c is the speed of light in vacuum. The electric field of the laser pulse is then $\mathbf{E} = -c^{-1}\partial \mathbf{A}/\partial t$ [37,38].

The nonuniformity (localization) of the field along the x axis drives evolution and spatial nonuniformity of the electron concentration in the sample, due to the action of the conductivity along the axis of the nanotubes, while the field nonuniformity along directions orthogonal to the axes of the nanotubes does not contribute to the redistribution of the electron concentration, due to negligible overlap of the wave functions of the electrons in adjacent nanotubes and the absence of conductivity in the (y, z) plane. Full analysis of the accumulation of electric charge and, accordingly, taking into account the field of this charge is a separate problem that is beyond the scope of this work. However, as shown by numerical simulations performed earlier (see Refs. [25–27]), differences in electron concentration (dynamic inhomogeneities) emerging in the course of the passage of electromagnetic pulses in the sample have the magnitude of few percent relative to the initial equilibrium concentration, n_0. In this case, there is no significant disturbance in the dynamics of the pulses with respect to the results obtained in the framework of the approximating admitting uniform field along the CNT axis (see, e.g., Ref. [22]). Thus, when considering ultrashort electromagnetic pulses, subject to the above-mentioned condition $\Delta t_{\text{pulse}} \ll t_{\text{rel}}$, the nonstationary disturbance in the concentration of conduction electrons may be neglected.

Based on these considerations, we assume that the distribution of the concentration of conduction electrons in the sample remains approximately constant, in accordance with the approximation of the uniform electric field acting in the axial direction. Thus, equations for the concentration of conduction electrons and scalar potential may be excluded from the system under the consideration. As a result, for the propagation of the short electromagnetic pulse through the CNT array, the evolution of the field in the array is described, with reasonable accuracy, by the single Eq. (2) for the vector potential.

The projection of the conduction current density j onto the CNT axis is determined using the approach developed in Refs. [39,40], which yields

$$j = 2e \sum_{s=1}^{m} \int_{-\pi\hbar/d}^{+\pi\hbar/d} v_x f(p_x, s) dp_x, \qquad (3)$$

where e is the electron charge ($e < 0$), v_x and $f(p_x, s)$ are the electron velocity and distribution function over quasimomenta p_x, and numbers s characterize, as said above, the quantization of the electron momentum along the perimeter of the nanotube. Factor 2 in Eq. (3) takes into account the summation of electrons over spins, and the integration over the quasimomentum is carried out within the first Brillouin zone. Using the expression for the energy of electrons (1) in determining their velocity $v_x = \partial\epsilon(p_x, s)/\partial p_x$, and taking into account the Fermi-Dirac distribution of electrons according to Eq. (3), we obtain an expression for the current density (further details of the derivation can be found in recent work [27]):

$$j = -en\frac{d_x}{\hbar}\gamma_0 \sum_{r=1}^{\infty} G_r \sin\left(rA\frac{ed_x}{c\hbar}\right). \qquad (4)$$

Here, n is the concentration of conduction electrons at a given point in the volume of the sample, and coefficients G_r are determined as

$$G_r = -r\frac{\sum_{s=1}^{m}\frac{\delta_{r,s}}{\gamma_0}\int_{-\pi}^{+\pi}\cos(r\theta)\left\{1 + \exp\left[\frac{\theta_{0,s}}{2} + \sum_{q=1}^{m}\theta_{q,x}\cos(q\theta)\right]\right\}^{-1}d\theta}{\sum_{s=1}^{m}\int_{-\pi}^{+\pi}\left\{1 + \exp\left[\frac{\theta_{0,s}}{2} + \sum_{q=1}^{m}\theta_{q,x}\cos(q\theta)\right]\right\}^{-1}d\theta}, \qquad (5)$$

where $\theta_{r,s} = \delta_{r,s}(k_B T)^{-1}$, k_B is the Boltzmann constant, T is temperature, and $\delta_{r,s}$ are coefficients of the expansion of electron energy (1) in the Fourier series [41],

$$\delta_{r,s} = \frac{d_x}{\pi\hbar}\int_{-\pi\hbar/d}^{+\pi\hbar/d}\epsilon(p_x, s)\cos\left(r\frac{d_x}{\hbar}p_x\right)dp_x. \qquad (6)$$

B. Introducing of the control high-frequency (HF) electric field

The presence of the field of the ultrashort pulse and external (control) HF electric field can be taken into account by replacing $A \to A + A_1$ in the expression for current density (4). Taking into regard the definition of the electric field, $\mathbf{E}_1 = \{E_1, 0, 0\} = -c^{-1}\partial\mathbf{A}_1/\partial t$, this replacement amounts to

$$A \to A - E_{10}\frac{c}{\omega_1}\sin(\omega_1 t + \alpha). \qquad (7)$$

Further, substituting Eq. (7) into expression (4) for the current density, and averaging the result over period $2\pi/\omega_1$ of the control HF electric field, we obtain an effective expression for the current density arising in the sample under the combined

action of both the short-pulse and control fields:

$$\langle j \rangle = -en\frac{d_x}{\hbar}\gamma_0 \sum_{r=1}^{\infty} J_0\left(r\frac{|eE_{10}|d_x}{\hbar\omega_1}\right)G_r \sin\left(rA\frac{ed_x}{c\hbar}\right), \quad (8)$$

where J_0 is the zeroth-order Bessel function [41] (see Appendix A for full details).

C. High-electron-density (HED) layer

An increase in the concentration of conduction electrons in a particular layer can be achieved, for example, by introducing donor dopants at the stage of fabrication of the sample (a detailed discussion of technical aspects of doping the CNT array by donors is beyond the scope of this theoretical paper). We stress that each segment of the sample is assumed to be electroneutral; in particular, in the HED layer, the larger charge density of free electrons is compensated by a balancing higher concentration of ionized dopants.

We assume that the HED layer is a region of thickness δz_{imp}, placed parallel to the CNT axes and perpendicular to the axis along which the ultrashort electromagnetic pulse propagates, see Fig. 1. We model the profile of the electron concentration in the sample by a natural Gaussian, cf. Ref. [31]:

$$n(z) = n^{\text{bias}} + \left(n_{\text{imp}}^{\text{max}} - n^{\text{bias}}\right)\exp\left\{-\left(\frac{z}{\delta z_{\text{imp}}}\right)^2\right\}, \quad (9)$$

where $n_{\text{imp}}^{\text{max}}$ is the maximum concentration of conduction electrons in the layer, and δz_{imp} is its half-width. The concentration of conduction electrons is assumed constant in any part of the (x, y) plane.

D. The effective equation for the vector potential

Substituting the expression for the conduction current density (8) into Eq. (2), and taking into account the electron concentration profile (9), we obtain the following effective equation for the evolution of the vector potential of the ultrashort pulse propagating through the CNT array, under the action of the control (external) HF field:

$$\frac{\partial^2 \Psi}{\partial \tau^2} - \frac{\partial^2 \Psi}{\partial \xi^2} - \frac{\partial^2 \Psi}{\partial \upsilon^2} - \frac{\partial^2 \Psi}{\partial \zeta^2}$$
$$+ \eta(\zeta)\sum_{r=1}^{\infty} J_0(\kappa r)G_r \sin(r\Psi) = 0. \quad (10)$$

The notation used in Eq. (10) is: $\Psi = (ed_x/c\hbar)A$ is the dimensionless projection of the vector potential of the ultrashort pulse onto the CNT axis;

$$\tau = \omega_0 t/\sqrt{\varepsilon}, \quad \xi = x\omega_0/c, \quad \upsilon = y\omega_0/c, \quad \zeta = z\omega_0/c \quad (11)$$

are dimensionless time and spatial coordinates; ε is the averaged relative dielectric constant of the sample (for further details, see Ref. [42]); $\eta(\zeta) = n/n^{\text{bias}}$ is the reduced distribution of the concentration of conduction electrons in the sample, calculated as per Eq. (9); and coefficients G_r are given by dimensionless expressions (5) that decrease with the

increase of r. Further, the quantity

$$\kappa = \frac{|eE_{10}|d_x}{\hbar\omega_1}, \quad (12)$$

characterizes the control HF electric field, and $\omega_0 = 2|e|d_x\hbar^{-1}(\pi n^{\text{bias}}\gamma_0)^{1/2}$ is a characteristic frequency of the electronic subsystem of CNTs. With parameters used in the paper (see below), it is $\approx \omega_0 = 7.14 \times 10^{12}\text{s}^{-1}$, corresponding to the vacuum wavelength $\lambda_0 = 264\,\mu\text{m}$, which belongs to the far-infrared domain. The central frequency of the waves under the consideration, typically determined by $1/\Delta t_{\text{pulse}}$, belong to the same range. As a consequence, high frequency ω_1 may be chosen in the midinfrared domain or even at the highest-frequency edge of the far-infrared band. Thus, Eq. (10) describes the evolution of the self-consistent field of an the ultrashort pulse interacting with the electronic subsystem of the CNT array, driven by control HF electromagnetic field.

IV. CHARACTERISTICS OF THE SHORT-PULSE'S FIELD

For illustrating the localization of the electromagnetic pulse in space, we will use the normalized electromagnetic energy density of the wave, $E^2 \equiv W(\xi, \upsilon, \zeta, \tau)$. Taking into account relation $\mathbf{E} = -c^{-1}\partial\mathbf{A}/\partial t$, the energy density of the field selected above can be represented as

$$W = W_0\left(\frac{\partial \Psi}{\partial \tau}\right)^2, \quad (13)$$

$$W_0 = E_0^2, \quad E_0 \equiv -\hbar\omega_0/(ed_x\sqrt{\varepsilon}). \quad (14)$$

When the electromagnetic pulse interacts with the HED layer, in the general case the incident pulse splits in transmitted and reflected wave packets. The ratio of their energies depends on various factors, including characteristics of the incident pulse, as well as parameters of the layer with an increased electron concentration [30–32]. As characteristics of the result of the interaction of the ultrashort pulse with the layer, we define transmission and reflection coefficients, following Refs. [31,32]:

$$K_{\text{pass}} = \frac{\int_0^{+\infty} d\zeta \int_{-\infty}^{+\infty} d\upsilon \int_{-\infty}^{+\infty} d\xi\, W(\xi, \upsilon, \zeta, \tau_\infty)}{\int_{-\infty}^{+\infty} d\zeta \int_{-\infty}^{+\infty} d\upsilon \int_{-\infty}^{+\infty} d\xi\, W(\xi, \upsilon, \zeta, \tau_\infty)}, \quad (15)$$

$$K_{\text{refl}} = \frac{\int_{-\infty}^{0} d\zeta \int_{-\infty}^{+\infty} d\upsilon \int_{-\infty}^{+\infty} d\xi\, W(\xi, \upsilon, \zeta, \tau_\infty)}{\int_{-\infty}^{+\infty} d\zeta \int_{-\infty}^{+\infty} d\upsilon \int_{-\infty}^{+\infty} d\xi\, W(\xi, \upsilon, \zeta, \tau_\infty)}, \quad (16)$$

where τ_∞ corresponds to any instant of time taken after completion of the interaction of the pulse with the layer, when the pulse is already located at a sufficiently large distance from the layer, and the field's energy density at the location of the layer is negligible in comparison to the maximum pulse's energy density. Coefficients K_{pass} and K_{refl}, defined by Eqs. (15) and (16) represent, severally, the ratio of the energy of the transmitted and reflected wave packets to the total field energy in the entire calculation region. The system considered in this paper being conservative, the coefficients are subject to relation $K_{\text{refl}} = 1 - K_{\text{pass}}$, which is a consequence of the energy conservation [43].

If the energy of the wave packet passing through the layer of the increased electron concentration substantially exceeds

the energy of the reflected wave packet ($K_{pass} \gg K_{refl}$), then the electromagnetic pulse passes through the layer. Otherwise, when the energy of the reflected wave packet substantially prevails over the energy of the transmitted one ($K_{pass} \ll K_{refl}$), this outcome is identified as the reflection of the electromagnetic pulse. At certain values of the system parameters, specifically, at the threshold value of the initial velocity of the incident pulse, it splits in two wave packets with approximately equal energies ($K_{pass} \approx K_{refl}$), which, after interacting with the layer of the increased electron concentration, propagate in opposite directions.

V. NUMERICAL RESULTS

A. Initial conditions: The shape of the ultrashort electromagnetic pulse

Equation (10) for the vector potential, which governs the evolution of the field of the ultrashort pulse in the inhomogeneous CNT array under the action of the control HF electric field, is a 3D generalization of the sine-Gordon equation. As it does not admit exact analytical solutions, we carried out numerical simulations, taking into account the electron density-distribution profile (9). Following the approach elaborated in previous works (see Ref. [32] and references therein), for the initial condition we take a product of the snapshot of the dimensionless projection $\Psi_\parallel(\zeta, \tau_0)$ of the field's vector potential onto the ξ axis of the CNTs at fixed time moment, $\tau = \tau_0$, and the initial distribution of the field in the (ξ, υ) plane, orthogonal to the propagation direction of the pulse:

$$\Psi(\xi, \upsilon, \zeta, \tau_0) = \Psi_\parallel(\zeta)\Psi_\perp(\xi, \upsilon). \tag{17}$$

We select the profile $\Psi_\parallel(\zeta, \tau_0)$ corresponding to the commonly known breather solution of the sine-Gordon equation [44],

$$\Psi_\parallel(\zeta, \tau) = 4 \arctan\left\{ \left(\frac{1}{\Omega^2} - 1\right)^{1/2} \frac{\sin \chi}{\cosh \mu} \right\}, \tag{18}$$

where

$$\chi = \sigma \Omega \frac{\tau(\zeta - \zeta_0)U}{\sqrt{1 - U^2}}, \tag{19}$$

$$\mu = \sigma\{\tau U - (\zeta - \zeta_0)\}\sqrt{\frac{1 - \Omega^2}{1 - U^2}}, \tag{20}$$

where $U = u/v$ is the ratio of the initial propagation velocity (19) of the pulse along the ζ axis to the speed of light in the medium, $v = c/\sqrt{\varepsilon}$; ζ_0 is the dimensionless coordinate of the center of mass of the pulse along the ζ axis at the time moment $\tau = \tau_0$; $\Omega \equiv \omega_B/\omega_0$, with self-oscillation frequency of the breather ω_B ($0 < \Omega < 1$); $\sigma \equiv \sqrt{G_1}$; and coefficients G_r are calculated using Eq. (5).

A Gaussian was chosen as the transverse profile of the pulse's field, which is adequate in many settings similar to the present one [45–47]:

$$\Psi_\perp(\xi, \upsilon) = \exp\left(-\frac{\xi^2 + \upsilon^2}{w_0^2}\right), \tag{21}$$

where w_0 is the initial transverse size of the pulse at $\tau = \tau_0$. Taking into regard Eqs. (18)–(21), the projection of the elec-

tric field strength of the pulse onto the CNT axis at $\tau = \tau_0$ is

$$E_x = E_{max} \frac{\cos \chi \cosh \mu - U(\Omega^{-2} - 1)^{1/2} \sin \chi \sinh \mu}{\cosh^2 \mu + (\Omega^{-2} - 1)\sin^2 \chi}$$
$$\times \exp\left(-\frac{\xi^2 + \upsilon^2}{w_0^2}\right), \tag{22}$$

where $E_{max} = 4E_0\sigma\sqrt{1 - \Omega^2}/\sqrt{1 - U^2}$.

The shape of the electromagnetic pulse generated by initial conditions (18)–(22) periodically changes. It is called bipolar because electric field (22) takes both positive and negative values. The characteristic duration of the pulse can be estimated as (cf. Ref. [32])

$$\Delta t_{pulse} = 2\frac{\ln(2 + \sqrt{3})}{\sigma \omega_0} \frac{\sqrt{\varepsilon}}{U} \frac{\sqrt{1 - U^2}}{\sqrt{1 - \Omega^2}}. \tag{23}$$

B. System's parameters

As an environment for modeling the propagation of the ultrashort electromagnetic pulse, we recall that we choose the CNT array of the zigzag type $(m, 0)$: $m = 7$, $\gamma_0 = 2.7$ eV, $b = 1.42 \times 10^{-8}$ cm, $d_x \approx 2.13 \times 10^{-8}$ cm, $n^{bias} = 10^{16}$ cm^{-3}, at temperature $T = 293$ K. We assume that the array is embedded in a dielectric matrix with the effective dielectric constant $\varepsilon = 4$ (see Ref. [32] and references therein).

Dimensionless parameter U [see Eqs. (19) and (20)] is varied within interval $U \in (0.5; 0.999)$. Extreme values $U > 0.999$ were not considered due to limitations imposed by the numerical scheme. On the other hand, at $U < 0.5$, the longitudinal width of the pulse begins to approach the value of the distance traveled by the pulse over a duration $\sim t_{rel}$, which is of no significant practical interest.

The dimensionless frequency Ω of internal oscillations of the initial pulse (18) was varied in interval $\Omega \in (0.1; 0.9)$. As Ω decreases, the width of the pulse along the ζ axis decreases too, the shape variation being insignificant at $\Omega < 0.5$. For $\Omega > 0.9$, the width becomes comparable to the distance traveled by the pulse over time $\sim t_{rel}$. Transverse width of the pulse was varied in the range of $1.0 \leqslant w_0 \leqslant 10.0$.

When modeling the profile of the electron concentration in the sample, we varied values of parameter $\eta_{imp}^{max} \equiv n_{imp}^{max}/n^{bias}$ that determines the maximum electron concentration in the inhomogeneity layer, see Eq. (9), in the range of $1 \leqslant \eta_{imp}^{max} \leqslant 100$. The dimensionless thickness of the HED layer, $\delta\zeta_{imp} = \delta z_{imp}\omega_0/c$, was varied in the range of 0.05–0.5. We stress that the use of the collisionless approximation (which makes it possible to consider the system as a conservative one) is justified if the evolution time is limited by the relaxation time t_{rel}. In particular, with $t_{rel} \approx 10$ ps, the ultrashort electromagnetic pulse travels distance $z \leqslant ct_{rel}/\sqrt{\varepsilon} \approx 0.15$ cm in the medium under the consideration.

C. Interaction of the ultrashort pulse with the high-electron-density (HED) layer

To solve Eq. (10) numerically with initial conditions (18)–(22), we used an explicit finite-difference three-layer cross-type scheme for hyperbolic equations described in Refs. [48,49] and adapted for the 3D model using the
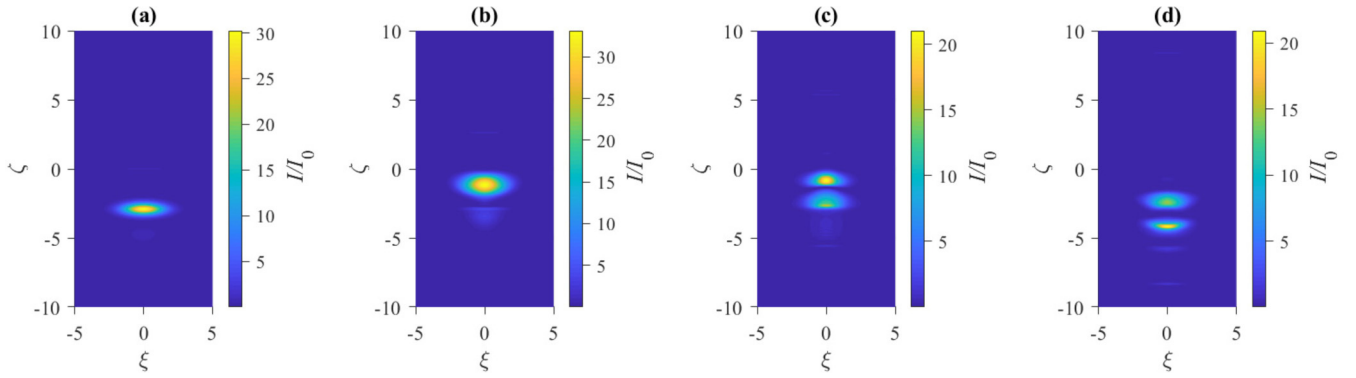
FIG. 2. Distribution of the field normalized energy density $W(\xi, 0, \zeta, \tau)$ in the CNT array, at various moments of dimensionless time $\tau = \omega_0 t / \sqrt{\varepsilon}$, in the case when the incident laser pulse is reflected from the high-electron-density (HED) layer, placed at $\zeta = 0$, in the absence of the control (external) HF field [$\kappa = 0$, see Eq. (12)]: (a) $\tau = 0$; (b) $\tau = 3.0$; (c) $\tau = 6.0$; (d) $\tau = 9.0$. The dimensionless coordinates are $\xi = x\omega_0/c$ and $\zeta = z\omega_0/c$ [see Eq. (11)]. The color code shows values of the energy density normalized as W/W_0 [see Eq. (14)], the yellow and blue areas corresponding to the maximum and minimum values of the field energy density, respectively.

approach reported in detail for the 2D setting in Ref. [31]. The calculations produced the electromagnetic field, $\Psi = \Psi(\xi, \upsilon, \zeta, \tau)$, and the respective field energy density was found as per Eq. (13).

It was thus found that, depending on values of the system's parameters, various scenarios of the interaction of the ultrashort electromagnetic pulse with the HED layer are possible, leading to the passage of the layer or reflection from it. The outcome is determined by control parameters, which are characteristics of the electromagnetic pulse itself (such as the speed of the incident pulse) and the layer (its thickness and the peak concentration of conduction electrons in it). The passage of the layer by the pulse is, naturally, enhanced by both the increase of the incidence speed and the decrease of the layer's thickness and electron concentration in it, cf. Ref. [32] and references therein. The reflection of short pulses from the HED has a simple explanation. With an increase in the concentration of carriers in the impurity band, the current induced by the incident pulse increases too. Thus, the impurity region becomes more conductive, in comparison to the homogeneous sample, and, as a consequence, more strongly reflects the electromagnetic wave [32]. On the other hand, a faster moving pulse has higher energy, which makes it is easier for it to overcome the effective potential barrier created by the HED layer [44].

Parameters of the waveguide medium are fixed by the manufacturing technology, therefore they cannot be changed to control the pulse-layer interaction. Parameters of the pulse may be altered, but applications may make it necessary to control the behavior of pulses with fixed parameters, created by standard sources. In this context, an essential option, developed in this work, is to change outcomes of the interaction by means of the control HF field, i.e., its amplitude and frequency may be used as efficient control parameters. In fact, the control effect may be achieved not only by varying these parameters, but also by turning the external field on/off. We present here results of modeling the propagation of short electromagnetic pulses in the inhomogeneous CNT array, for fixed parameters of the pulse and HED layer, both in the absence or presence of the control HF field.

Figures 2 and 3 display the interaction of the ultrashort electromagnetic pulse with the HED layer for various values of strength κ [see Eq. (12)] of the control HF field and fixed values of the initial pulse's parameters $\Omega = 0.5$ and $w_0 = 2.0$. In this case, the maximum value of the electric field of the pulse is $|E_x|_{\max} \approx 6.1 \times 10^5$ V/cm [see Eq. (22)], and its duration is $\Delta t_{\text{pulse}} \approx 0.67$ ps, see Eq. (23). For the definiteness, we have selected the following fixed values of parameters of the HED layer: $\eta_{\text{imp}}^{\max} = 30$ and $\delta \zeta_{\text{imp}} = 0.1$.

Figures 2 and 3 display the distribution of the field energy density of the ultrashort pulse, $W(\xi, 0, \zeta, \tau)$, see Eq. (13), in the (ξ, ζ) plane (at $\upsilon = 0$) at various moments of the dimensionless time, $\tau = \omega_0 t / \sqrt{\varepsilon}$. The normalized field energy density is represented by colored-coded values of W/W_0, with W_0 defined as per Eq. (14). The horizontal and vertical dimensionless coordinates are $\xi = x\omega_0/c$ and $\zeta = z\omega_0/c$, which are defined above in Eq. (11). With the values of the system's parameters selected above, $\xi = 1$ and $\zeta = 1$ correspond to distance $\approx 4.2 \times 10^{-3}$ cm. Note that in these figures we present the distribution of the energy density only in the (ξ, ζ) plane (at $\upsilon = 0$), as it is identical to that in the (υ, ζ) plane.

Figure 2 shows an example of the reflection of the ultrashort electromagnetic pulse from the HED layer in the absence of the control HF field ($\kappa = 0$). The initial pulse's speed is taken as $U = 0.8$, which corresponds to the initial speed $u = 0.012$ cm/ps in physical units. In this case, the transmission and reflection coefficients, defined by Eqs. (15) and (16), are found to be $K_{\text{pass}} \approx 0.0143$ and $K_{\text{refl}} \approx 0.9857$, respectively, confirming the nearly complete reflection of the incident pulse (small-amplitude transmitting waves are not visible in Fig. 2).

Figure 3 shows the opposite situation, *viz.*, the passage of the pulse, with the same parameters as in Fig. 2, through the same HED layer, in the presence of the control HF field with amplitude $E_{10} = 5.8 \times 10^6$ V/cm and frequency $\omega_1 = 9.4 \times 10^{13}$ s^{-1}, which corresponds to $\kappa \approx 2.0$, as per Eq. (12). In this case, the transmission and reflection coefficients are $K_{\text{pass}} \approx 0.9196$ and $K_{\text{refl}} \approx 0.0804$, respectively, which confirms the practically complete passage, with a small reflected wave being virtually invisible in Fig. 3. Note that, at $\kappa \approx 2.0$, significantly stronger diffraction spreading of the pulse is
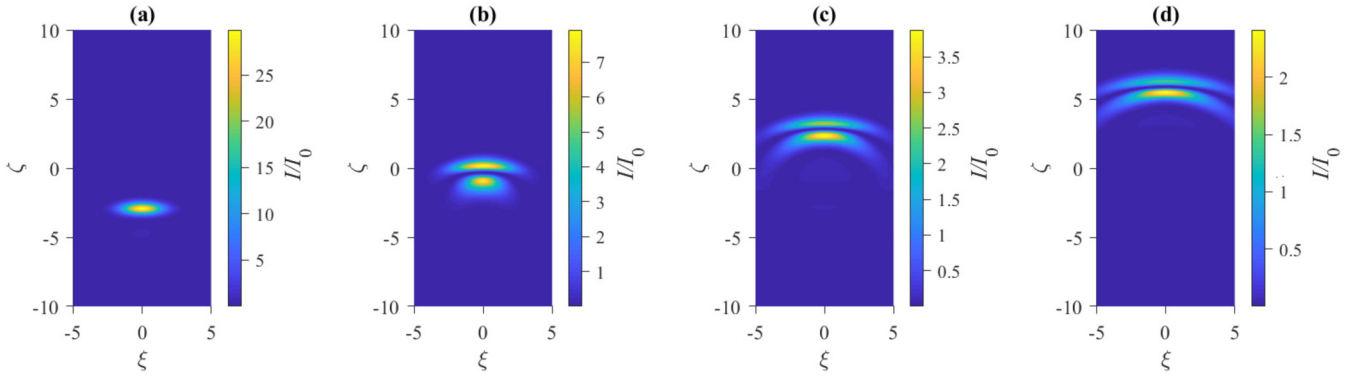
FIG. 3. The same as in Fig. 2, but for the case when the incident pulse passes the HED layer, in the presence of the control HF field, with strength $\kappa = 2.0$ [see Eq. (12)]: (a) $\tau = 0$; (b) $\tau = 3.0$; (c) $\tau = 6.0$; (d) $\tau = 9.0$.

observed, in comparison to the case shown in Fig. 2, as in present case the pulse propagates in the medium with properties of the electronic subsystem dynamically modified by the control HF field, therefore self-focusing properties of this medium are less pronounced in comparison with the case of $\kappa = 0$.

Figure 4 shows dependencies of the reflection and transmission coefficients K_{pass} and K_{refl} on initial speed U, longitudinal width and duration (for a fixed value of strength κ of the control HF field), and on κ (for a fixed value of U). As can be seen in Fig. 4(a), the transmission and reflection coefficients increase and decrease, respectively, with the increase of velocity U, cf. Ref. [32]. When the initial velocity of the incident ultrashort pulse significantly exceeds a certain threshold value, $U \gg U_{thr}$, the passage of the pulse through the HED layer prevails over the reflection. At $U = U_{thr}$ the transmission and reflection coefficients are equal, $K_{refl}(U_{thr}) \approx K_{pass}(U_{thr}) = 1/2$, with the incident pulse splitting in two approximately identical wave packets, one of which continues to move in the original direction, while the other one bounces back. Figure 4(a) shows that, with the increase of strength κ of

the control HF field, the threshold velocity U_{thr} shifts to lower values. In other words, the control field upholds the passage of the short pulse through the HED layer.

In Fig. 4(b), the coefficients become equal, $K_{pass} = K_{refl}$, at strength κ of the control field equal to the respective threshold value, κ_{thr}. A noteworthy result, clearly seen in the figure, is that K_{pass} and K_{refl} vary nonmonotonously as functions of κ at $\kappa > \kappa_{thr}$. In particular, the reflection coefficient features almost zero values at its local minima, which may be considered as transparency windows of the medium for the propagation of the ultrashort electromagnetic pulses.

Using Eq. (8), and taking into account the fact that, in a rough approximation, all G_r with $r \neq 1$ can be neglected, the current in the absence of HF field can be expressed as

$$\langle j \rangle \approx -en\frac{d_x}{\hbar}\gamma_0 J_0\left(r\frac{|eE_{10}|d_x}{\hbar\omega_1}\right)G_1 \sin\left(rA\frac{ed_x}{c\hbar}\right), \quad (24)$$

i.e., due to the electronic properties of the CNTs, it is a periodic function of the vector potential. The external HF field acts as a phase shift in this periodic function. Only the mean value of the current over the fast oscillations has an effect on
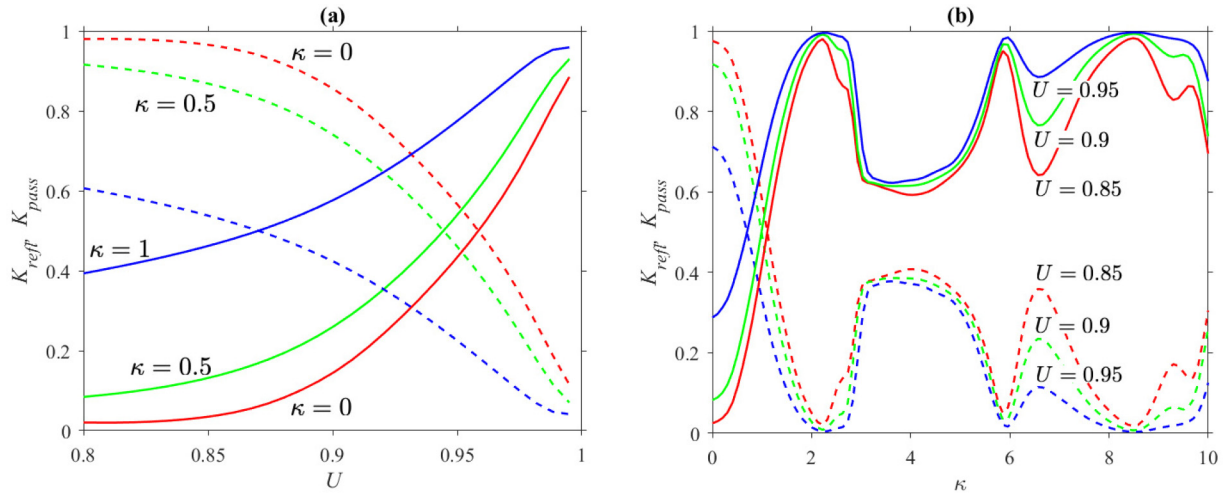

FIG. 4. (a) The transmission and reflection coefficients, K_{pass} and K_{refl} (the solid and dashed lines, respectively) as functions of the initial speed U of the incident electromagnetic pulse, for fixed values of strength κ of the control field attached to each curve. (b) The same coefficients as functions of κ, at fixed values of U attached to the curves. In both panels, marked are threshold values U_{thr} and κ_{thr}, at which the transmission and reflection coefficients are equal.
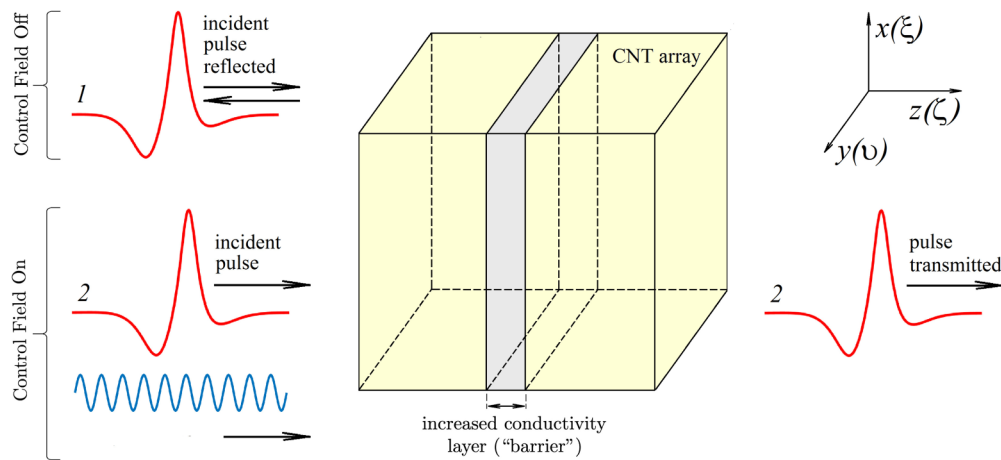
FIG. 5. The schematic of a soliton valve, based on the HED layer embedded in the CNT array. (*1*) In the absence of the control HF field, the incident pulse is reflected by the barrier layer. (*2*) The application of the control field unlocks the barrier, letting the pulse pass through it.

the infrared pulse propagation but, due to this dependence, this mean value vanishes for specific values of the HF field intensity only (unless either the infrared pulse or the HF field strongly dominates). These values correspond to a specific value of the parameter κ, which can be defined as the ratio of two energies, say $\kappa = W_{CNT}/W_{HF}$, where $W_{CNT} = E_{10}ed_x$ is the typical magnitude of the energy of the electric dipolar momentum of the CNT in the HF field, and $W_{HF} = \hbar\omega_1$ the energy of the HF field photon. The transparency windows appear thus as a resonant effect, which occurs when the photon energy matches the energy of the CNT dipolar momentum.

This effect resembles the phenomenon of the electromagnetically induced transparency (EIT) [33–35,50–53], where the photonic resonance is the key factor. The main difference between the problem under consideration and the problem with EIT is that the EIT effect is observed in an environment in which an electromagnetic field propagates in a medium considered as a set of discrete well-separated energy levels of atoms. In our case, the electromagnetic field propagates within the medium of electrons located in the conduction band (or holes in the valence band) of the carbon nanotubes. The spectrum in our case is continuous. We also note that the EIT effect leads to a deceleration of the pulse of the electromagnetic field. This is achieved by saturating the population at certain levels (depending on the level scheme). In the present study, given the continuity of the spectrum, the concept of saturation is irrelevant, and, accordingly, the pulse does not slow down as in the EIT problems.

The location of the windows on the scale of κ may be explained by rewriting current (8) in terms of κ, taking into account that, in a rough approximation, all G_r with $r \neq 1$ can be neglected, and, with regard to Eq. (12), the result is:

$$\langle j \rangle \approx -en\frac{d_x}{\hbar}\gamma_0 J_0(\kappa)G_1 \sin\left(A\frac{ed_x}{c\hbar}\right). \qquad (25)$$

Indeed, it is easy to see that bottom points of the windows in Fig. 4(b) are relatively close to zeros of function $J_0(\kappa)$ in Eq. (25). Actually, the Bessel factor $J_0(\kappa)$ represents the result of the above-mentioned resonance effect.

Because the nonlinearity nearly vanishes in Eq. (10) in the region of the transparency windows, dynamics of the

ultrashort pulse becomes nearly linear in such cases. This fact explains the spatiotemporal evolution in Fig. 3, in the course of the passage through the HED layer, the pulse undergoes noticeable transverse and longitudinal deformation due to diffraction and dispersion, which is characteristic for the propagation in quasilinear media. On the contrary, the deformation is not prominent in Fig. 2, which pertains to the case of strong nonlinearity.

Thus, the result of the interaction of the short laser pulse with the HED layer depends on the values of several parameters, among which a special role is played by the amplitude and frequency of the control HF field, which may be used as the most effective control parameters of the system, as they may be varied without changing the sample's structure and/or standard pulses employed by the scheme. In particular, these parameters may be efficiently used to change, as required, the threshold velocity of the incident pulse, U_{thr}, which separates the reflection and passage outcomes of the collision of the pulse with the HED barrier.

A conclusion is that the scheme elaborated here may be used as a soliton valve, somewhat similar to the concept of all-optical transistors (light controlled by light) [54,55]. An illustration is presented in Fig. 5: while, in the absence of the control HF field, the HED layer does not let the incident short pulse pass the barrier, one can open the passage by applying the control field with appropriate values of the amplitude and frequency.

VI. CONCLUSIONS

This study reports four key results, which may have far-reaching practical applications in the area of design and development of optoelectronic systems. First, we establish that, as a result of the interaction of the ultrashort electromagnetic pulse with the barrier layer of high electron density (HED) in an array of carbon nanotubes (CNTs), the pulse can either pass through the layer or be reflected from it. This first result is important as it offers the possibility to effectively use variable HED layers to achieve specific propagation or reflection of ultrashort pulses.

Second, our analysis of this rich phenomenon reveals that the collision of the pulse with the HED layer exhibits a very particular dependence on both the parameters of the pulse and the properties of the HED layer itself. Specifically, we found that an increase of the speed and amplitude of the incident pulse facilitates the passage of the pulse through this layer. This property paves the way to a particular modulation of the pulse through its speed and amplitude in order to control its penetration effectiveness.

Third, we establish the central result of this study, which is built upon the two previous key results. It has been found that the state of the electronic subsystem in the CNT array may be controlled by an external HF field. That control field may be used to facilitate the passage of the ultrashort pulse through the barrier layer, thereby creating transparency windows around particular values of the control field's amplitude. This effect, based in the resonant effect of the HF fields, is similar to the phenomenon of the electromagnetically induced transparency.

Lastly, and from the practical standpoint, we proved that the latter effect can be used for the design of a soliton valve, which allows one to efficiently switch the system between the reflection and transmission regimes for the soliton stream, without changing its parameters, but rather adjusting the amplitude and frequency of the control field.

APPENDIX A: DETAILED DERIVATION OF EQ. (8)

This Appendix provides a detailed derivation of Eq. (8):

$$j = -en\frac{d_x}{\hbar}\gamma_0 \sum_{r=1}^{\infty} J_0\left(r\frac{|eE_{10}|d_x}{\hbar\omega_1}\right)G_r \sin\left(rA\frac{ed_x}{c\hbar}\right).$$

As a starting point, we replace A by $(A + A_1)$ inside the term $\sin(rA\frac{ed_x}{c\hbar})$ in Eq. (4). As specified by Eq. (7), this amounts to replacing A by $A - E_{10}\frac{c}{\omega_1}\sin(\omega_1 t + \alpha)$ in the rightmost sine term in Eq. (8):

$$\sin\left(rA\frac{ed_x}{c\hbar}\right) \rightarrow \sin\left[r\left(A - E_{10}\frac{c}{\omega_1}\sin(\omega_1 t + \alpha)\right)\frac{ed_x}{c\hbar}\right], \tag{A1}$$

with

$$\sin\left[r\left(A - E_{10}\frac{c}{\omega_1}\sin(\omega_1 t + \alpha)\right)\frac{ed_x}{c\hbar}\right] = \sin\left(rA\frac{ed_x}{c\hbar}\right)\cos(\rho\sin\beta) - \cos\left(rA\frac{ed_x}{c\hbar}\right)\sin(\rho\sin\beta), \tag{A2}$$

where the following two quantities have been introduced to simplify the notations:

$$\rho = rE_{10}\frac{c}{\omega_1}\frac{ed_x}{c\hbar}, \tag{A3}$$

$$\beta = \omega_1 t + \alpha. \tag{A4}$$

Using Bessel functions of the first kind, one can obtain that

$$\cos(\rho\sin\beta) = J_0(\rho) + 2\sum_{k=1}^{\infty} J_{2k}(\rho)\cos(2k\beta), \tag{A5}$$

$$\sin(\rho\sin\beta) = 2\sum_{k=1}^{\infty} J_{2k-1}(\rho)\sin[(2k-1)\beta], \tag{A6}$$

where J_μ is the μth order Bessel function of the first kind [41]. Substituting these last two equations into Eq. (A2), and subsequently in Eq. (4), we obtain the expression for the electric current density

$$j = -en\frac{d_x}{\hbar}\gamma_0 \Bigg\{ \sum_{r=1}^{\infty} G_r \sin\left(rA\frac{ed_x}{c\hbar}\right)J_0\left(rE_{10}\frac{c}{\omega_1}\frac{ed_x}{c\hbar}\right) + 2\sum_{r=1}^{\infty}\sum_{k=1}^{\infty} G_r \sin\left(rA\frac{ed_x}{c\hbar}\right)J_{2k}\left(rE_{10}\frac{c}{\omega_1}\frac{ed_x}{c\hbar}\right)\cos[2k(\omega_1 t + \alpha)]$$

$$+ 2\sum_{r=1}^{\infty}\sum_{k=1}^{\infty} G_r \cos\left(rA\frac{ed_x}{c\hbar}\right)J_{2k-1}\left(rE_{10}\frac{c}{\omega_1}\frac{ed_x}{c\hbar}\right)\sin[(2k-1)(\omega_1 t + \alpha)] \Bigg\}. \tag{A7}$$

As a next step, we average the electric current density j in Eq. (A7) over the period $T_1 = 2\pi/\omega_1$ of the high-frequency external electric field and obtain the desired equation:

$$\langle j \rangle = -en\frac{d_x}{\hbar}\gamma_0 \sum_{r=1}^{\infty} J_0\left(r\frac{|eE_{10}|d_x}{\hbar\omega_1}\right)G_r \sin\left(rA\frac{ed_x}{c\hbar}\right). \tag{A8}$$

[1] E. A. Khazanov, S. Yu. Mironov, and G. Mourou, Nonlinear compression of high-power laser pulses: compression after compressor approach, Phys. Usp. **62**, 1096 (2019).

[2] M. Kolesik and J. V. Moloney, Modeling and simulation techniques in extreme nonlinear optics of gaseous and condensed media, Rep. Prog. Phys. **77**, 016401 (2014).

[3] Y. Yin, X. Ren, A. Chew, J. Li, Y. Wang, F. Zhuang, Y. Wu, and Z. Chang, Generation of octave-spanning mid-infrared pulses from cascaded second-order nonlinear processes in a single crystal, Sci. Rep. **7**, 11097 (2017).

[4] A. Couairon, J. Biegert, C. P. Hauri, W. Kornelis, F. W. Helbing, U. Keller, and A. Mysyrowicz, Self-compression of ultra-short laser pulses down to one optical cycle by filamentation, J. Mod. Opt. **53**, 75 (2006).

[5] B. A. Malomed, D. Mihalache, F. Wise, and L. Torner, Spatiotemporal optical solitons, J. Opt. B: Quantum Semicl. Opt. **7**, R53 (2005).

[6] H. Leblond and D. Mihalache, Models of few optical cycle solitons beyond the slowly varying envelope approximation, Phys. Rep. **523**, 61 (2013).

[7] S. V. Sazonov and N. V. Ustinov, Propagation of few-cycle pulses in a nonlinear medium and an integrable generalization of the sine-Gordon equation, Phys. Rev. A **98**, 063803 (2018).

[8] N. N. Konobeeva and M. B. Belonenko, Influence of initial shape of three-dimensional few-cycle optical pulse on its propagation in topological insulator thin films, Rom. Rep. Phys. **70**, 403 (2018).

[9] B. A. Malomed and D. Mihalache, Nonlinear waves in optical and matter-wave media: A topical survey of recent theoretical and experimental results, Rom. J. Phys. **64**, 106 (2019).

[10] D. Mihalache, Multidimensional localized structures in optical and matter-wave media: A topical survey of recent literature, Rom. Rep. Phys. **69**, 403 (2017).

[11] I. Babushkin, A. Tajalli, H. Sayinc, U. Morgner, G. Steinmeyer, and A. Demircan, Simple route toward efficient frequency conversion for generation of fully coherent supercontinua in the mid-IR and UV range, Light: Sci. Appl. **6**, e16218 (2017).

[12] A. B. Aceves, C. De Angelis, A. M. Rubenchik, and S. K. Turitsyn, Multidimensional solitons in fiber arrays, Opt. Lett. **19**, 329 (1994).

[13] A. Geim, Graphene: Status and Prospects, Science **324**, 1530 (2009).

[14] F. Bonaccorso, Z. Sun, T. Hasan, and A. C. Ferrari, Graphene photonics and optoelectronics, Nat. Photonics **4**, 611 (2010).

[15] A. V. Eletskii, Carbon nanotubes, Phys. Usp. **40**, 899 (1997).

[16] R. H. Baughman, A. A. Zakhidov, and W. A. de Heer, Carbon nanotubes–the route toward applications, Science **297**, 787 (2002).

[17] Y. Segawa, H. Ito, and K. Itami, Structurally uniform and atomically precise carbon nanostructures, Nature Rev. Mater. **1**, 15002 (2016).

[18] M. B. Belonenko, S. Yu. Glazov, and N. E. Meshcheryakova, Nonlinear conductivity of single-walled zigzag carbon nanotubes, Bull. Russ. Acad. of Sci.: Phys. **73**, 1601 (2009).

[19] A. V. Zhukov, R. Bouffanais, M. B. Belonenko, and E. G. Fedorov, Propagation of laser beams in an array of semiconductor carbon nanotubes, Mod. Phys. Lett. B **27**, 1350045 (2013).

[20] M. B. Belonenko and E. G. Fedorov, Self-focusing of super-Gaussian laser beams propagating in an array of carbon nanotubes, Russ. Phys. J. **55**, 436 (2012).

[21] M. B. Belonenko, E. V. Demushkina, and N. G. Lebedev, Electromagnetic solitons in a system of carbon nanotubes, J. Russ. Laser Res. **27**, 457 (2006).

[22] E. G. Fedorov, A. V. Zhukov, M. B. Belonenko, and T. F. George, 2D electromagnetic breathers in carbon nanotubes, Eur. Phys. J. D **66**, 219 (2012).

[23] H. Leblond and D. Mihalache, Spatiotemporal optical solitons in carbon nanotube arrays, Phys. Rev. A **86**, 043832 (2012).

[24] E. G. Fedorov, A. V. Pak, and M. B. Belonenko, Interaction of two-dimensional electromagnetic breathers in an array of carbon nanotubes, Phys. Sol. State **56**, 2112 (2014).

[25] M. B. Belonenko and E. G. Fedorov, Extremely short electromagnetic pulses in an array of carbon nanotubes with a longitudinal field inhomogeneity, Phys. Sol. State **55**, 1333 (2013).

[26] A. V. Zhukov, R. Bouffanais, E. G. Fedorov, and M. B. Belonenko, Three-dimensional electromagnetic breathers in carbon nanotubes with the field inhomogeneity along their axes, J. Appl. Phys. **114**, 143106 (2013).

[27] A. V. Zhukov, R. Bouffanais, B. A. Malomed, H. Leblond, D. Mihalache, E. G. Fedorov, N. N. Rosanov, and M. B. Belonenko, Collisions of three-dimensional bipolar optical solitons in an array of carbon nanotubes, Phys. Rev. A **94**, 053823 (2016).

[28] E. G. Fedorov, N. N. Konobeeva, and M. B. Belonenko, Two-dimensional electromagnetic breathers in an array of nanotubes with multilevel impurities, Russ. J. Phys. Chem. B **8**, 409 (2014).

[29] M. Belonenko, A. Popov, and N. Lebedev, Dynamics of laser bullet propagation in carbon nanotube array with metal inhomogeneities, Tech. Phys. Lett. **37**, 119 (2011).

[30] A. V. Zhukov, R. Bouffanais, E. G. Fedorov, and M. B. Belonenko, Interaction of a two-dimensional electromagnetic breather with an electron inhomogeneity in an array of carbon nanotubes, J. Appl. Phys. **115**, 203109 (2014).

[31] A. V. Zhukov, R. Bouffanais, H. Leblond, D. Mihalache, E. G. Fedorov, and M. B. Belonenko, Interaction of a two-dimensional electromagnetic pulse with an electron inhomogeneity in an array of carbon nanotubes in the presence of field inhomogeneity, Eur. Phys. J. D **69**, 242 (2015).

[32] E. G. Fedorov, A. V. Zhukov, R. Bouffanais, A. P. Timashkov, B. A. Malomed, H. Leblond, D. Mihalache, N. N. Rosanov, and M. B. Belonenko, Propagation of three-dimensional bipolar ultrashort electromagnetic pulses in an inhomogeneous array of carbon nanotubes, Phys. Rev. A **97**, 043814 (2018).

[33] O. Kocharovskaya and Ya. I. Khanin, Coherent population trapping and the attendant effect of absorptionless propagation of ultrashort pulse trains in a three-level medium, Zh. Eksp. Teor. Fiz. **90**, 1610 (1986) [English translation: Sov. Phys. JETP **63**, 945 (1986)].

[34] Y. Rostovtsev, O. Kocharovskaya, G. R. Welch, and M. O. Scully, Slow, ultraslow, stored, and frozen light, Opt. Phot. News **13**, 44 (2002).

[35] M. Fleischhauer, A. Imamoglu, and J. P. Marangos, Electromagnetically induced transparency: Optics in coherent media, Rev. Mod. Phys. **77**, 633 (2005).

[36] R. A. Jishi, M. S. Dresselhaus, and G. Dresselhaus, Electrophonon coupling and the electrical conductivity of fullerene nanotubules, Phys. Rev. B **48**, 11385 (1993).

[37] L. D. Landau, E. M. Lifshitz, and L. P. Pitaevskii, *Electrodynamics of Continuous Media*, 2nd ed. (Elsevier, Oxford, 2004).

[38] L. D. Landau and E. M. Lifshitz, *The Classical Theory of Fields*, 4th ed. (Butterworth-Heinemann, Oxford, 2000).

[39] E. M. Epshtein, Solitons in a superlattice, Fiz. Tverd. Tela **19**, 3456 (1976).

[40] E. M. Epshtein, Drag of electrons by solitons in a semiconductor superlattice, Fiz. Tech. Polupr. **14**, 2422 (1980) [Sov. Phys. Semiconductors **14**, 1438 (1980)].

[41] G. A. Korn and T. M. Korn, *Mathematical Handbook for Scientists and Engineers* (McGraw Hill, New York, 1968).

[42] F. G. Bass, A. A. Bulgakov, and A. P. Tetervov, *High Frequency Properties of Semiconductors with Superlattices* (Nauka, Moscow, 1989).

[43] J. D. Jackson, *Classical electrodynamics* (John Wiley & Sons, New York, 2007).

[44] Yu. S. Kivshar and B. A. Malomed, Dynamics of solitons in nearly integrable systems, Rev. Mod. Phys. **61**, 763 (1989).

[45] C. Rulliére, Ed., *Femtosecond Laser Pulses: Principles and Experiments* (Springer-Verlag, Berlin, 1998).

[46] A. N. Pikhtin, *Optical and Quantum Electronics* (High School Publishers, Moscow, 2001).

[47] D. S. Simon, *A Guided Tour of Light Beams* (Morgan & Claypool Publishers, Williston, 2016).

[48] S. E. Koonin, *Computational Physics: Fortran Version* (Ingram Publisher Services, Boulder, 1998).

[49] J. W. Thomas, *Numerical Partial Differential Equations - Finite Difference Methods* (Springer-Verlag, New York, 1995).

[50] S. E. Harris, J. E. Field, and A. Imamoglu, Nonlinear Optical Processes Using Electromagnetically Induced Transparency, Phys. Rev. Lett. **64**, 1107 (1990).

[51] K.-J. Boller, A. Imamoglu, and S. E. Harris, Observation of Electromagnetically Induced Transparency, Phys. Rev. Lett. **66**, 2593 (1991).

[52] A. Kasapi, M. Jain, G. Y. Yin, and S. E. Harris, Electromagnetically Induced Transparency: Propagation Dynamics, Phys. Rev. Lett. **74**, 2447 (1995).

[53] M. G. Payne and L. Deng, Consequences of induced transparency in a double-Lambda scheme: Destructive interference in four-wave mixing, Phys. Rev. A **65**, 063806 (2002).

[54] M. F. Yanik, S. H. Fan, M. Soljačić, and J. D. Joannopoulos, All-optical transistor action with bistable switching in a photonic crystal cross-waveguide geometry, Opt. Lett. **28**, 2506 (2003).

[55] D. Ballarini, M. De Giorgi, E. Cancellieri, R. Houdre, E. Giacobino, R. Cingolani, A. Bramati, G. Gigli, and D. Sanvitto, All-optical polariton transistor, Nature Commun. **4**, 1778 (2013).